Electrocatalysis Hot Paper

International Edition: DOI: 10.1002/anie.201910662
German Edition: DOI: 10.1002/ange.201910662

Highly Selective Production of Ethylene by the Electroreduction of Carbon Monoxide

*Ruixue Chen[+], Hai-Yan Su[+], Deyu Liu, Rui Huang, Xianguang Meng, Xiaoju Cui, Zhong-Qun Tian, Dong H. Zhang, and Dehui Deng**

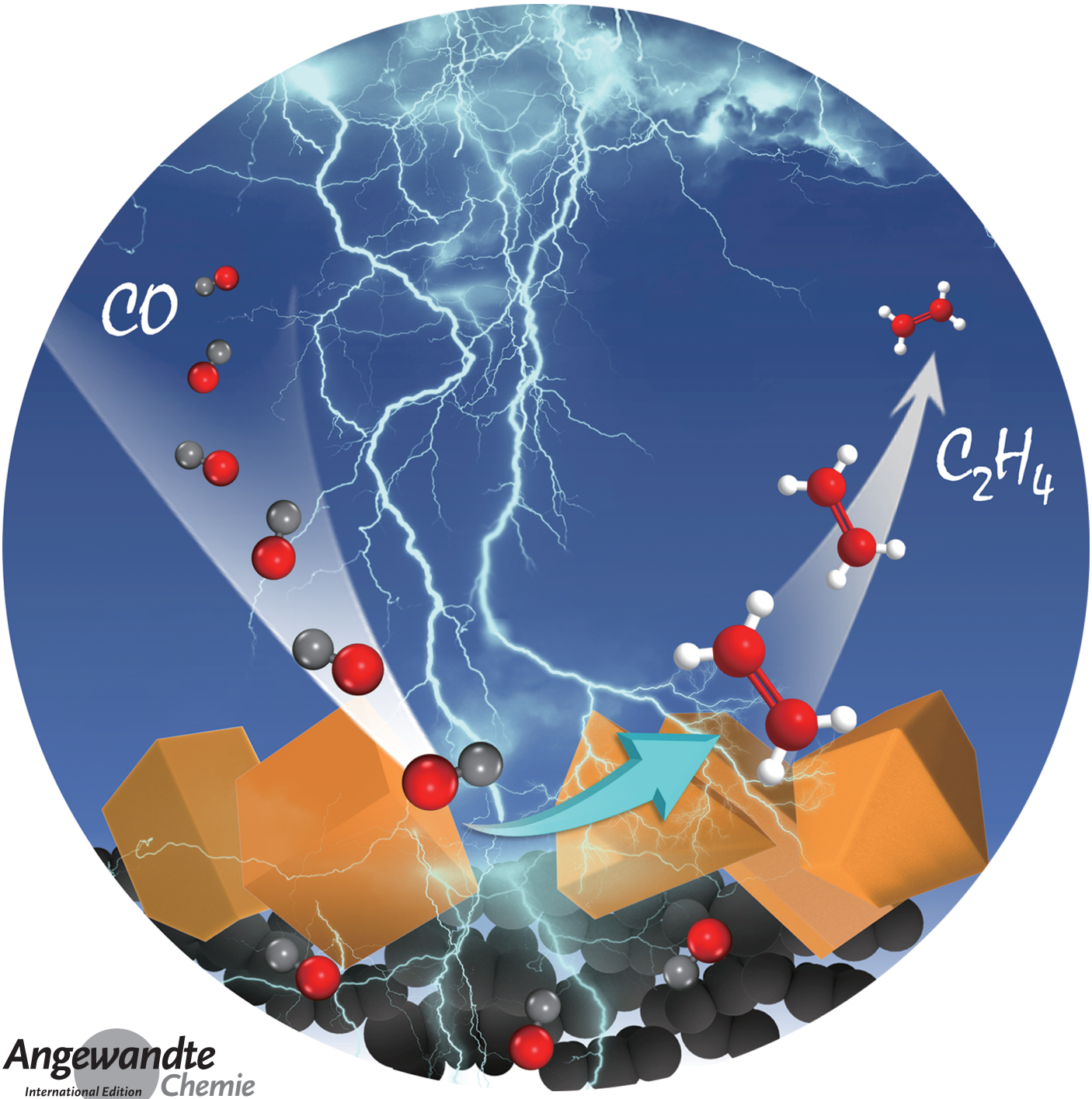

Abstract: *Conversion of carbon monoxide to high value-added ethylene with high selectivity by traditional syngas conversion process is challenging because of the limitation of Anderson-Schulz–Flory distribution. Herein we report a direct electrocatalytic process for highly selective ethylene production from CO reduction with water over Cu catalysts at room temperature and ambient pressure. An unprecedented 52.7% Faradaic efficiency of ethylene formation is achieved through optimization of cathode structure to facilitate CO diffusion at the surface of the electrode and Cu catalysts to enhance the C–C bond coupling. The highly selective ethylene production is almost without other carbon-based byproducts (e.g. C_1–C_4 hydrocarbons and CO_2) and avoids the drawbacks of the traditional Fischer–Tropsch process that always delivers undesired products. This study provides a new and promising strategy for highly selective production of ethylene from the abundant industrial CO.*

Ethylene (C_2H_4) is an important building block for the chemical industry and usually produced by steam cracking of naphtha feedstocks at 800–900 °C. However, considering the utilization of the nonpetroleum carbon resources, converting an abundant industrial carbon resource, such as CO from syngas ($CO + H_2$), into C_2H_4 through an energy-efficient strategy is regard as a key process. Over the years, much attention has been attracted by C_2–C_4 olefin production by the Fischer–Tropsch synthesis (FTS) under high temperatures (200–450 °C) and high pressures (5–50 bar).[1] Apart from these harsh reaction conditions and consuming hydrogen resources, the products from the FTS process are often limited by the Anderson–Schulz–Flory (ASF) distribution, which leads to 30% selectivity of C_2 hydrocarbons (ethylene and ethane) at most.[2] The resultant gas mixture containing C_1–C_4 hydrocarbons requires further separation to get high-purity ethylene.[2b,3] In addition, there is still as much as 30–50% CO_2 selectivity accompanying the products of the FTS into olefins,[2b,3a–c] which causes undesired carbon emission and carbon loss. Therefore, the development of highly selective and energy-saving ethylene production routes without additional separation and waste of carbon resources is of great industrial, economic, and environmental interest.

[*] R. Chen,[+] Prof. D. Liu, Dr. X. Cui, Prof. Z.-Q. Tian, Prof. D. Deng
Collaborative Innovation Center of Chemistry for Energy Materials, College of Chemistry and Chemical Engineering, Xiamen University
Xiamen 361005 (China)
R. Chen,[+] Prof. R. Huang, Prof. X. Meng, Dr. X. Cui, Prof. D. Deng
State Key Laboratory of Catalysis, Collaborative Innovation Center of Chemistry for Energy Materials, Dalian Institute of Chemical Physics, Chinese Academy of Sciences
Dalian 116023 (China)
E-mail: dhdeng@dicp.ac.cn
Prof. H.-Y. Su,[+] Prof. D. H. Zhang
State Key Laboratory of Molecular Reaction Dynamics, Dalian Institute of Chemical Physics, Chinese Academy of Sciences
Dalian 116023 (China)
[+] These authors contributed equally to this work.
Supporting information and the ORCID identification number(s) for the author(s) of this article can be found under: https://doi.org/10.1002/anie.201910662.

In contrast to the electrocatalytic systems, cracking of naphtha and FTS to olefins both suffer from high energy consumption and a complex processes of product separation. Electrocatalytic systems with spatially separated oxidation and reduction processes allow for a different reaction equilibrium and product selectivity via designing special electrodes in electrolytes at mild conditions. Taking advantage of a rationally designed anode, recently we have succeeded in high-purity hydrogen production via an electrochemical water-gas shift reaction at room temperature.[4] This success inspires us to adopt an electrocatalytic strategy for another reaction, that is, the electrocatalytic CO reduction to ethylene (CORTE) process. Electrocatalytic CO reduction has emerged as a promising approach to attain multi-carbon alcohols[5] with a high energy conversion efficiency. However, the direct electrocatalytic CORTE process had rarely been reported,[5] a result of the low Faradaic efficiency (FE) and selectivity of ethylene.

Herein we report a highly selective and efficient production of ethylene from electrocatalytic CO reduction with water at room temperature and ambient pressure. Through rational optimization of polytetrafluoroethylene (PTFE) content to increase the CO concentration at the surface of electrode and the Cu particle catalysts to enhance the C–C bond coupling, this electrocatalytic CORTE process can achieve an unprecedentedly high ethylene FE of 52.7%. Moreover, the high selectivity of ethylene production without any CO_2 emission breaks through the 30% selectivity limitation from CO to C_2 hydrocarbons in traditional FTS process, which always delivers uncontrollable mixture of C_1–C_4 hydrocarbons and massive CO_2.

The low solubility of CO in electrolyte leads to the low local concentration of CO on the surface of catalysts, which therefore limits the efficiency of the electrocatalytic CORTE process. It is believed that increasing the hydrophobicity of the electrode surface can reduce the affinity of water to the electrode and promote the diffusion of CO to the water-electrode interface. Besides, the carbon papers themselves are inert in CO electroreduction reaction (Figure S1 in Supporting Information). Hence, carbon papers with different hydrophobicity (CP-5%, CP-13%, CP-25%, and CP-MPL) were selected as the supports of Cu particles (Cu-Ps) to optimize the CO diffusion on the surface of Cu-Ps. The amounts of PTFE of CP-5%, CP-13% and CP-25% are 5 wt%,13 wt% and 25 wt%, respectively. CP-MPL is composed of hydrophobic carbon fiber and 25% PTFE treatment micro-porous layer (MPL) while other three types of carbon paper are without MPL.

The electrocatalytic CORTE process is greatly affected by the hydrophobicity and porous structure of catalyst supports. As shown in Figure 1 a and Figure S2, with the hydrophobicity increasing from CP-5% to CP-MPL reflected by their contact angle, the corresponding FE of C_2H_4 will increase from 2.46% to 52.7%. It suggests that the high hydrophobicity of electrode is one of the key factors to enhance CO conversion into C_2H_4. Moreover, the geometric current density of C_2H_4 (j_{C2H4}) over Cu-Ps/CP-MPL is 2-fold as that of Cu-Ps/CP-25% when the amounts of PTFE in both samples is 25 wt%. It indicates that micro-porous layer (MPL) structure is another

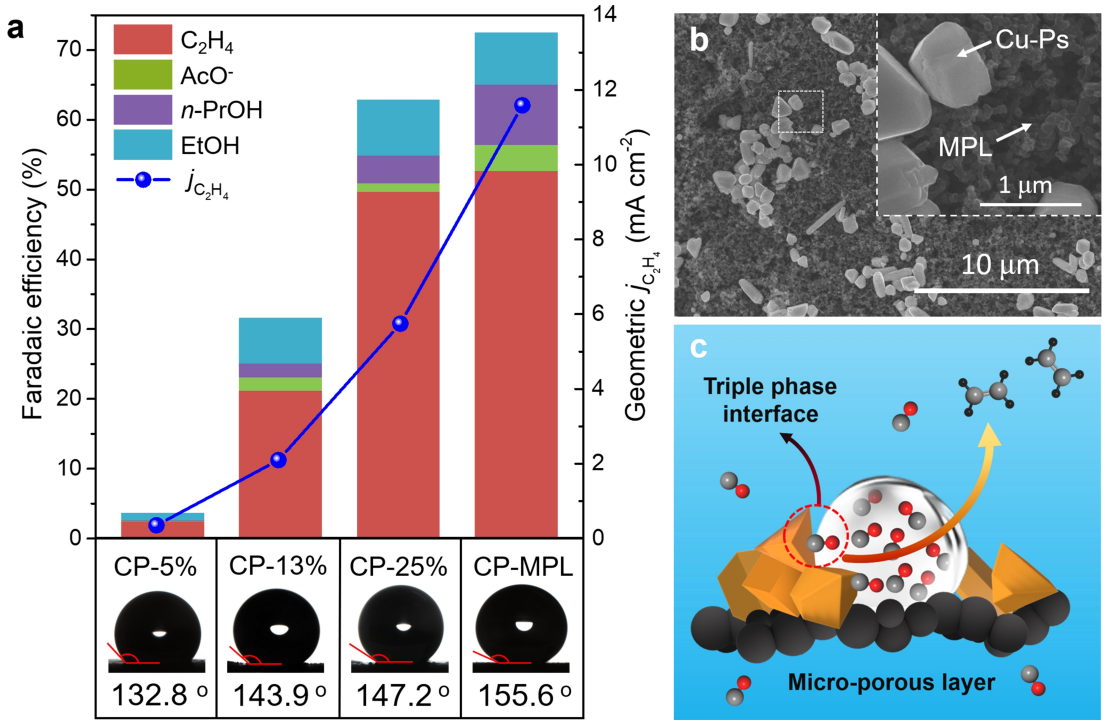

Figure 1. Electrode structure and the related CORTE performance. a) Faradaic efficiency and geometric current density for CO electroreduction over Cu-Ps loaded on four types of carbon papers tested in 1 M KOH at 25 °C. Bottom pictures show contact angles of water droplets on the corresponding surface of carbon papers. b) SEM images of Cu-Ps/CP-MPL electrode. c) Schematic illustration for CORTE process on Cu catalysts with the assistant of the hydrophobic micro-porous layer to improve the CO diffusion.

key factor to enhance the reaction rate of CORTE. Accordingly, scanning electron microscopy (SEM) images (Figure 1b) show Cu-Ps/CP-MPL electrode has a special granular micro-porous structure (around 100 nm). This micro-porous structure of Cu-Ps/CP-MPL can efficiently increase the CO diffusion at the interface of gas/liquid/solid as depicted in Figure 1c which is similar with the report where CO_2 electroreduction is enhanced by using carbon paper with MPL.[6] Compared with CP-MPL, carbon paper without MPL (Figure S3) does not favor the construction of three-phase interface. Besides, the C_2H_4 production performance of Cu-Ps on carbon papers with higher PTFE content was also tested (Figure S4). However, the activity slightly decreases with PTFE increasing to 35 wt%. It is probably caused by a reduction in the conductivity of electrode at higher PTFE content, which is in agreement with the conductivity test reported by Kenis et al.[6b] Thus, optimizing the hydrophobicity and micro-porous layer structure of carbon paper provides an efficient strategy to construct hydrophobic microenvironment in gas/liquid/solid interfaces, which enhances the diffusion of CO molecules and the corresponding electrocatalytic CORTE process.

Since initial oxidation state of copper-based catalysts plays key role in CO/CO_2 electroreduction,[7] in particular for yielding multi-carbon oxygenates, it is unclear whether the oxidation state of initial catalysts benefits CORTE process. Then three typical copper-based samples were selected as catalysts to examine the initial oxidation-state effect of copper on the CORTE reactions, including Cu-Ps catalyst, copper oxide (CuO-syn) synthesized by an oxidation procedure of Cu-Ps, and commercial copper oxide (CuO). As shown in Figure 2b, the samples of both CuO-*syn* and CuO share similar X-ray diffraction (XRD) patterns containing copper oxide phase, whereas the freshly prepared Cu-Ps has a face-centered cubic copper phase. During the CO electroreduction process, there are hydrogen and five carbon-based products detected on the cathode including ethylene, ethanol (EtOH), acetate (AcO^-), *n*-propanol (*n*-PrOH) and trace amount of methane (Figure S5 and Table S1).

Comparisons of data in Figure 2a clearly show that the Cu-Ps delivers the highest C_2H_4 formation FE and total CO electroreduction FE among all three samples. Correspondingly, the geometric current density of C_2H_4 production over Cu-Ps is larger than that over CuO-syn (except at −0.9 V) and commercial CuO (Figure 2c). In addition, geometric current density (Figure 2c) and the intrinsic activity normalized by electrochemical surface area (ECSA, see Figure S6 for more details) of three catalysts are similar at −0.4 V and −0.5 V. However, the C_2H_4 FE of CuO-syn are much like that of Cu-Ps at lower potentials (less negative than −0.6 V). It implies that the electrocatalytic CORTE performance is recovered to some extent when CuO-syn is mostly in situ reduced into metallic copper at lower potentials as evidenced by XRD (Figure 2b). This result suggests that the oxidized copper could make against the CORTE reaction and the metallic copper should be the real active species for CORTE process. The optimal FE of C_2H_4 and total FE of CO electroreduction over Cu-Ps can reach 52.7% and 72.5% at −0.7 V in 1M

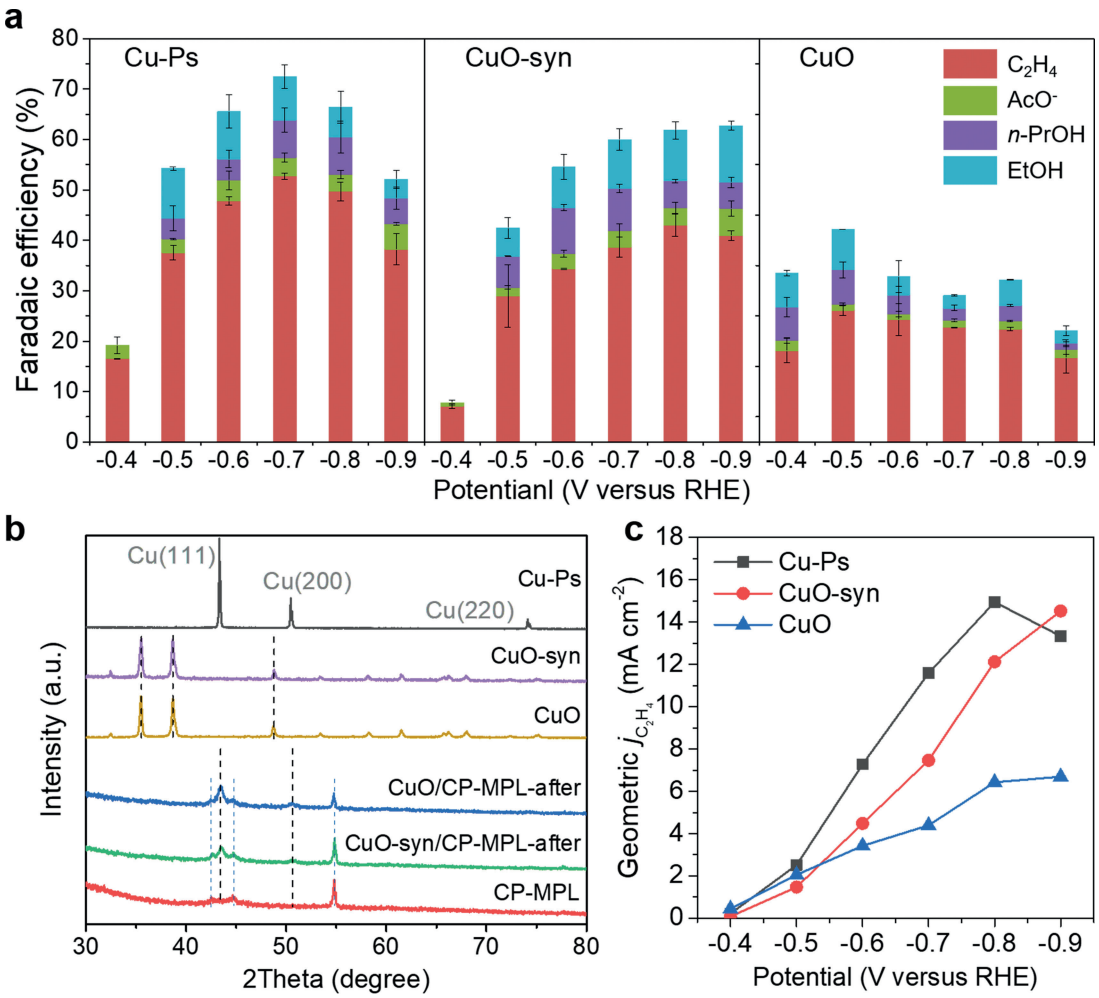

Figure 2. Copper oxidation-state effect on CORTE performance. a) Faradaic efficiencies of products over different Cu-based catalysts at applied potentials versus the reversible hydrogen electrode (RHE) in 1 M KOH at 25 °C. b) XRD patterns of freshly prepared catalysts and that after 2 hours CO electroreduction process at −0.7 V versus RHE (conditions: 1 M KOH, 25 °C). c) Geometric current densities for C_2H_4 production over different copper-based catalysts.

KOH, respectively. Ethylene is the only hydrocarbon product from CO electroreduction at wide potentials. Besides, a small amount of liquid products including EtOH, AcO^-, and *n*-PrOH are concomitantly generated, which are widely considered as value-added products and will not influence the separation of ethylene gas in practice. To our knowledge, the FE of C_2H_4 is unprecedented in comparison to all previous reports of CO electroreduction listed in Table S2, which could benefit from both the excellent catalytic performance of Cu-Ps and the hydrophobic micro-porous structure of the electrode.

Apart from the effect of electrode structure and initial oxidation-state of copper-based catalysts, we find that the OH^- concentration also has an important influence on the performance of electrocatalytic CORTE over Cu-Ps. As shown in Figure 3, the highest geometric current density of CORTE increases from 7.2 mA cm^{-2} to 22.4 mA cm^{-2} with increasing the concentration of KOH electrolyte from 0.1 M to 3 M, and the total geometric current density correspondingly has a two-fold increase at all potentials. One possible reason of reaction rate enhancement is that increasing OH^- concentration can accelerate the ion migration in aqueous electrolyte. The increasing FE of CO electroreduction with the increasing concentration of OH^- is possibly caused by inhibiting the competitive hydrogen evolution in higher pH (Figure S7), leading to more reaction sites for CO reduction and a higher FE of C–C coupling reaction. The selectivity of C_2H_4 reaches the highest value in 1M KOH at −0.7 V while the high the concentration of OH^- in favor of higher selectivity of AcO^- at all tested potentials. Besides, the selectivity based on CO conversion to ethylene (Figure S8) is around 70% (in 1M KOH), breaking through the 30% selectivity limitation from CO to C_2 hydrocarbons in traditional FTS process. Through optimizing the OH^- concentration together with the catalyst and the electrode structure, we can achieve a C_2H_4 FE of up to 52.7% with a geometric current density of 14.9 mA cm^{-2} in 1M KOH at −0.7 V. Besides, the Cu-Ps also has a good stability within 24 hours during CORTE process (Figure S9).

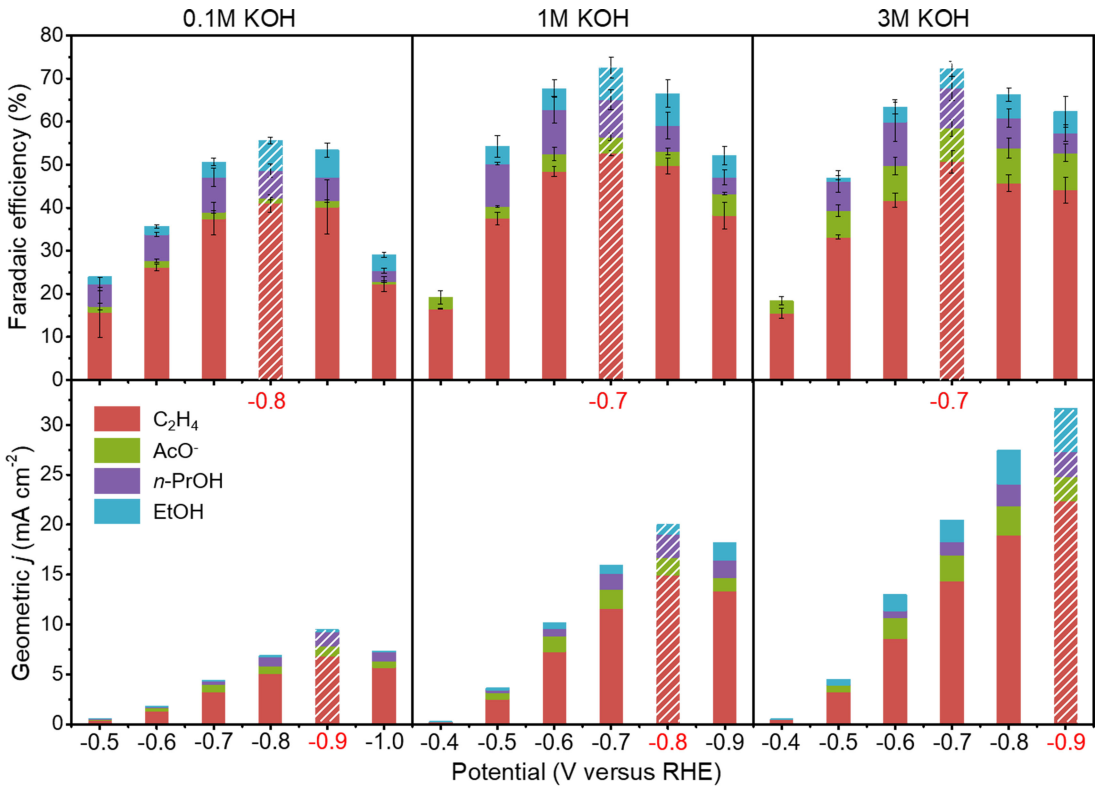

Figure 3. OH^- concentration effect on the performance of CORTE. Faradaic efficiencies (top) and geometric current densities (bottom) over Cu-Ps for CO electroreduction to C_2H_4, EtOH, AcO^- and *n*-PrOH at applied potentials versus RHE. Reaction temperature: 25 °C. KOH concentration: 0.1, 1, 3 M. The potential value highlighted in red on the bottom of each panel corresponds to the optimal value of each condition, respectively.

For better understanding the nature of CO electroreduction reaction, the in situ X-ray absorption spectroscopy (XAS) experiment and density functional theory (DFT) simulations were carried out. As shown in Figure 4a,b, the X-ray absorption near-edge structure (XANES) and extended X-ray absorption fine structure (EXAFS) spectra both prove that the catalyst keeps the metallic copper during the CO electroreduction reaction. Note that the peak for the Cu–Cu bond of Cu-Ps becomes higher after applying negative potentials comparing with the initial catalyst (Figure 4b), which may be caused by the reduction of the surface oxide layer on the Cu particles during the reaction. It further demonstrates that the metallic Cu should be the active phase for the CORTE process, which provides the basis for constructing the DFT model. Then we investigated the reaction mechanism of electrochemical reduction of CO on three Cu surfaces (111), (100) and (110) by using DFT calculations.

The key intermediates and favorable reaction pathways in the present work are shown in Figure 4c (see Figures S10,S11 for more intermediates and pathways investigation). Figure 4d and Figures S12,S13 show the free energy diagrams on Cu(100), Cu(111), and Cu(110). It can be seen that formation of the C_2O_2* is the most endergonic electrochemical step and determines the overpotentials of the cathode reaction, which follows the order 0.89 V on Cu(111) > 0.70 V on Cu(110) > 0.21 V on Cu(100). As shown in Figure 4e, the high activity of Cu(100) may originate from its stronger binding with C_2O_2* relative to 2 CO* (by 0.92 eV). Since Cu(111) and Cu(110) are unfavorable to yield C_2O_2* intermediate, we only investigate the C_2O_2* coupling with CO* for the formation of *n*-PrOH (Figure 4c and Figures S11f and S11g) on Cu(100). The step is endothermic by 0.57 eV, indicating that the C_3 product is not preferred to be formed on the Cu single crystalline surfaces.

The proton–electron transfer of CHCOH* splits the pathway to C_2H_4 from the pathway to EtOH. The competitive CCH* and CHCHOH* formation largely determines the selectivity of C_2H_4 and EtOH on the three surfaces (Figure 4d and Figures S12,S13). As seen from Figure 4e, CCH* formation is thermodynamically more favorable than CHCHOH* formation by 0.32 eV on Cu(100), which therefore results in the higher selectivity towards C_2H_4 than EtOH. On Cu(111), the two competitive steps have equivalent ΔG, suggesting similar selectivity towards C_2H_4 and CH_3CH_2OH. However, CHCHOH* instead of CCH* is preferred to be formed (by 0.17 eV) on Cu(110), which indicates a higher selectivity towards EtOH. The structure dependent selectivity may be due to the distinct water arrangement on the Cu surfaces.[8] Cu(110) prefers the five-membered ring of water molecules, which is more sparse than the six-membered ring arrangement on Cu(100) and Cu(111), thereby stabilizing the adsorption of large CHCHOH* intermediates by 0.67 and 0.35 eV compared to other two Cu surfaces.

In addition, we also investigated the CH_3COOH selectivity, which is few addressed in the literatures. Following previous work,[9] we studied the pathway via CH_2COHO* and

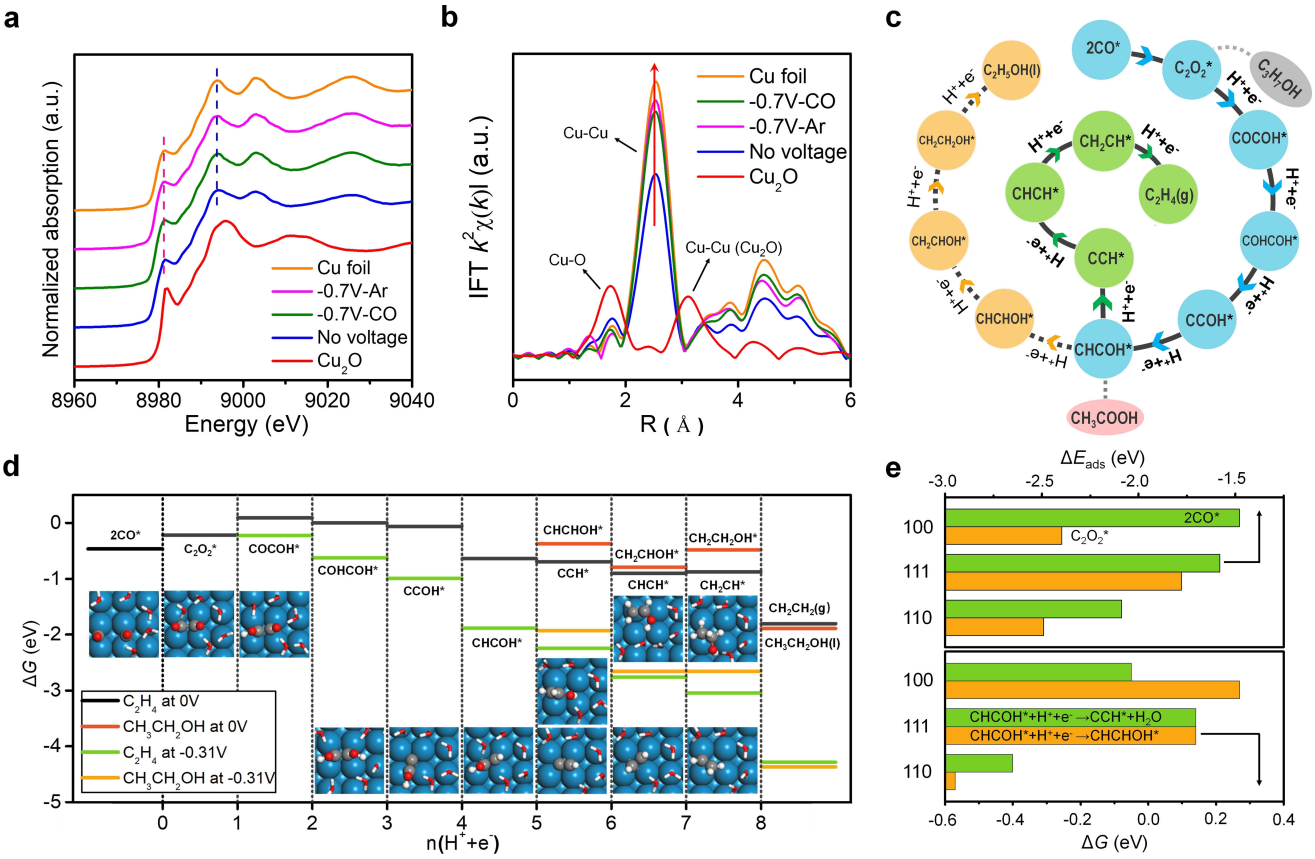

Figure 4. Insights into the reaction mechanism towards CO electroreduction on the Cu surfaces. a),b) The in situ normalized a) Cu K-edge XANES spectra and b) Cu K-edge k^2-weighted EXAFS spectra of Cu-Ps for no voltage and at −0.7 V in CO or Ar compared with the reference Cu foil and Cu_2O. c) Schematic representations of CO electroreduction reaction pathways. d) Free energy diagram for CO electroreduction on Cu(100) at $U=0$ V, and at the potentials that all the reaction steps are exothermic except for the first step. e) The adsorption energy of key intermediates that affect activity (upper panel) and free energies of competitive pathways for C_2H_4 and EtOH formation (lower panel) on Cu(100), Cu(111), and Cu(110).

(HO)(CH_2)OC* (see Figure S14 for more details) intermediates. However, no stable structures are identified on Cu(100) in water environment. Based on the consideration of both activity and selectivity as shown above, Cu(100) is the most preferred surface for C_2H_4 formation. This agrees with the results of online electrochemical mass spectroscopy experiments reported previously where Cu single crystals were used as the model catalysts to explore the active sites.[10] Thus, it could be speculated that exposed {100} planes in Cu-Ps dominate the performance of CORTE process.

In summary, we report a direct and efficient electrocatalytic process by using the Cu particle catalysts to enhance the CO conversion into ethylene at room temperature and atmospheric pressure. Through optimizing the structure of gas diffusion electrode, the intrinsic activity of the Cu-based catalyst, and the OH^- concentration, we achieve an ultrahigh CORTE performance with the C_2H_4 Faradaic efficiency of up to 52.7%. Theoretical calculations considering all possible products suggest that Cu(100) is the most preferred plane for C_2H_4 formation. This electrocatalytic CORTE process provides a more selective, energy-efficient, and eco-friendly way to convert the abundantly industrial CO into C_2H_4 than the Fischer–Tropsch synthesis process.

Acknowledgements

We gratefully acknowledge the financial support from the Ministry of Science and Technology of China (No. 2016YFA0204100, 2017YFA0204800 and 2016YFA0200200), the National Natural Science Foundation of China (No. 21890753, 21988101 and 21872136), the Key Research Program of Frontier Sciences of the Chinese Academy of Sciences (No. QYZDB-SSW-JSC020), and the DNL Cooperation Fund, CAS (No. DNL180201). We thank the staff at the BL14W1 beamline of the Shanghai Synchrotron Radiation Facilities for assistance with the EXAFS and XANES measurements. We thank Pengyang Zhang (Xiamen University) for assistance in contact angle tests.

Conflict of interest

The authors declare no conflict of interest.

Keywords: CO reduction · Cu catalyst · electrocatalysis · ethylene production · heterogeneous catalysis

How to cite: *Angew. Chem. Int. Ed.* **2020**, *59*, 154 – 160
Angew. Chem. **2020**, *132*, 160 – 166

[1] a) H. M. Torres Galvis, K. P. de Jong, *ACS Catal.* **2013**, *3*, 2130 – 2149; b) K. Cheng, J. C. Kang, D. L. King, V. Subramanian, C. Zhou, Q. H. Zhang, Y. Wang, *Adv. Catal.* **2017**, *60*, 125 – 208.

[2] a) G. Henrici-Olivé, S. Olivé, *Angew. Chem. Int. Ed. Engl.* **1976**, *15*, 136 – 141; *Angew. Chem.* **1976**, *88*, 144 – 150; b) F. Jiao, X. L. Pan, K. Gong, Y. X. Chen, G. Li, X. H. Bao, *Angew. Chem. Int. Ed.* **2018**, *57*, 4692 – 4696; *Angew. Chem.* **2018**, *130*, 4782 – 4786.

[3] a) F. Jiao, J. J. Li, X. L. Pan, J. P. Xiao, H. B. Li, H. Ma, M. M. Wei, Y. Pan, Z. Y. Zhou, M. R. Li, S. Miao, J. Li, Y. F. Zhu, D. Xiao, T. He, J. H. Yang, F. Qi, Q. Fu, X. H. Bao, *Science* **2016**, *351*, 1065 – 1068; b) L. S. Zhong, F. Yu, Y. L. An, Y. H. Zhao, Y. H. Sun, Z. J. Li, T. J. Lin, Y. J. Lin, X. Z. Qi, Y. Y. Dai, L. Gu, J. S. Hu, S. F. Jin, Q. Shen, H. Wang, *Nature* **2016**, *538*, 84; c) H. M. Torres Galvis, J. H. Bitter, C. B. Khare, M. Ruitenbeek, A. I. Dugulan, K. P. de Jong, *Science* **2012**, *335*, 835 – 838; d) Y. Yao, D. J. Graziano, M. Riddle, J. Cresko, E. Masanet, *Ind. Eng. Chem. Res.* **2016**, *55*, 3493 – 3505.

[4] X. Cui, H. Y. Su, R. Chen, L. Yu, J. Dong, C. Ma, S. Wang, J. Li, F. Yang, J. Xiao, M. Zhang, D. Ma, D. Deng, D. H. Zhang, Z. Tian, X. Bao, *Nat. Commun.* **2019**, *10*, 86.

[5] a) Y. Hori, A. Murata, R. Takahashi, S. Suzuki, *J. Am. Chem. Soc.* **1987**, *109*, 5022 – 5023; b) Y. Hori, R. Takahashi, Y. Yoshinami, A. Murata, *J. Phys. Chem. B* **1997**, *101*, 7075 – 7081; c) C. W. Li, J. Ciston, M. W. Kanan, *Nature* **2014**, *508*, 504 – 507; d) D. Raciti, L. Cao, K. J. T. Liv, P. F. Rottmann, X. Tang, C. Y. Li, Z. Hicks, K. H. Bowen, K. J. Hemker, T. Mueller, C. Wang, *ACS Catal.* **2017**, *7*, 4467 – 4472; e) Y. X. Wang, D. Raciti, C. Wang, *ACS Catal.* **2018**, *8*, 5657 – 5663; f) M. Jouny, W. Luc, F. Jiao, *Nat. Catal.* **2018**, *1*, 748 – 755; g) E. Bertheussen, T. V. Hogg, Y. Abghoui, A. K. Engstfeld, I. Chorkendorff, I. E. L. Stephens, *ACS Energy Lett.* **2018**, *3*, 634 – 640; h) L. H. Han, W. Zhou, C. X. Xiang, *ACS Energy Lett.* **2018**, *3*, 855 – 860; i) T.-T. Zhuang, Y. Pang, Z.-Q. Liang, Z. Wang, Y. Li, C.-S. Tan, J. Li, C. T. Dinh, P. De Luna, P.-L. Hsieh, T. Burdyny, H.-H. Li, M. Liu, Y. Wang, F. Li, A. Proppe, A. Johnston, D.-H. Nam, Z.-Y. Wu, Y.-R. Zheng, A. H. Ip, H. Tan, L.-J. Chen, S.-H. Yu, S. O. Kelley, D. Sinton, E. H. Sargent, *Nat. Catal.* **2018**, *1*, 946 – 951; j) Y. J. Pang, J. Li, Z. Y. Wang, C. S. Tang, P. L. Hsieh, T. T. Zhuang, Z. Q. Liang, C. Q. Zou, X. Wang, P. De Luna, J. P. Edwards, Y. Xu, F. W. Li, C. T. Dinh, M. Zhong, Y. H. Lou, D. Wu, L. J. Chen, E. H. Sargent, D. Sinton, *Nat. Catal.* **2019**, *2*, 251 – 258.

[6] a) D. Kopljar, A. Inan, P. Vindayer, N. Wagner, E. Klemm, *J. Appl. Electrochem.* **2014**, *44*, 1107 – 1116; b) B. Kim, F. Hillman, M. Ariyoshi, S. Fujikawa, P. J. A. Kenis, *J. Power Sources* **2016**, *312*, 192 – 198.

[7] a) C. S. Le Duff, M. J. Lawrence, P. Rodriguez, *Angew. Chem. Int. Ed.* **2017**, *56*, 12919 – 12924; *Angew. Chem.* **2017**, *129*, 13099 – 13104; b) D. F. Gao, I. Zegkinoglou, N. J. Divins, F. Scholten, I. Sinev, P. Grosse, B. Roldan Cuenya, *ACS Nano* **2017**, *11*, 4825 – 4831.

[8] J. Carrasco, A. Michaelides, M. Forster, S. Haq, R. Raval, A. Hodgson, *Nat. Mater.* **2009**, *8*, 427 – 431.

[9] a) Y. W. Lum, T. Cheng, W. A. Goddard, J. W. Ager, *J. Am. Chem. Soc.* **2018**, *140*, 9337 – 9340; b) A. J. Garza, A. T. Bell, M. Head-Gordon, *ACS Catal.* **2018**, *8*, 1490 – 1499.

[10] a) F. S. Roberts, K. P. Kuhl, A. Nilsson, *ChemCatChem* **2016**, *8*, 1119 – 1124; b) E. Pérez-Gallent, G. Marcandalli, M. C. Figueiredo, F. Calle-Vallejo, M. T. M. Koper, *J. Am. Chem. Soc.* **2017**, *139*, 16412 – 16419.

Manuscript received: August 21, 2019
Revised manuscript received: October 8, 2019
Accepted manuscript online: November 7, 2019
Version of record online: December 3, 2019

